THE AMERICAN SOCIETY OF MECHANICAL ENGINEERS
345 E. 47 St., New York, N.Y. 10017

93-WA/APM-17

Dynamic Holographic-Electronic Speckle-Pattern Interferometry

M. A. Ahmadshahi[1]

Sridhar Krishnaswamy[2]
Assoc. Mem. ASME.

S. Nemat-Nasser
Fellow ASME.

Center of Excellence for Advanced Materials,
Department of Applied Mechanics
and Engineering Sciences,
University of California, San Diego,
La Jolla, CA 92093-0411

The development of a nondestructive, full-field, quantitative optical technique, and its feasibility to study dynamic deformations of opaque and diffusively reflecting solids under transient loads, are discussed. The technique involves recording a sequence of dynamically changing two-beam speckle interference patterns (also called holographic speckle patterns) of a rapidly deforming body which is doubly illuminated by a laser light source. The time sequence of speckle patterns is recorded by means of a high-speed camera on an ultra-sensitive 35-mm film. The developed negatives are then digitized by a CCD camera into an image processing system. An initial speckle pattern corresponding to the undeformed state of the object is taken as the reference, and subsequent speckle patterns are digitally subtracted (reconstructed) from it to produce time-varying fringe patterns corresponding to the relative deformation of the test object. In order to gain confidence that the technique can be used to record truly transient deformation, it is tested here on a vibrating plate at resonance, thereby obtaining the evolution of the fringe pattern during 1/2 cycle of deformation corresponding to 160 μs.

1 Introduction

Optical techniques such as holographic and speckle interferometry provide means by which one can obtain full-field, quantitative measurements of deformations of objects under different loading conditions. The nondestructive nature of such techniques makes them suitable for use in hostile environments where other types of probes may be damaged, or may interfere with the implementation of the experiment, rendering them ineffective.

Speckle patterns are random intensity distributions, produced by a coherent light source, such as a laser, as it illuminates a diffusely reflecting body (Dainty, 1975). There are two types of fundamentally different speckle patterns; holographic speckle patterns which contain both phase and amplitude information simultaneously; and photographic speckle patterns which contain information pertaining only to the amplitude of the lightwave. In the latter case, the speckle patterns are obtained when a diffuse surface of an object is illuminated by a single coherent beam and the resulting scattered wavefront is recorded on a photographic emulsion medium. A double exposure of such speckle photographs, one exposure taken before and another taken after deformation of the object, is then illuminated by laser beams at discrete points to generate the corresponding Young's fringes, used to quantify the displacement components. Considerable effort has been devoted to this type of speckle-pattern photography, and detailed studies can be found in Francon (1979). Holographic speckle patterns, on the other hand, are obtained when the scattered wavefront emanating from the diffuse surface of the object is recorded simultaneously with a reference wavefront on the photographic emulsion medium. The speckle pattern recorded in the original experiment of Gabor's in-line holography (Gabor, 1948), leading to the hologram of the object, is an example of a holographic speckle pattern. Holographic interferometry is, in essence, the interference of two recorded holographic speckle patterns. Two such speckle patterns, corresponding to the undeformed and deformed state of the object, are recorded on the same photographic emulsion medium, hence involving double-exposure holography. The addition of these intensity variations produces fringe patterns that are directly related to the displacement of the object (Solid, 1969). Cartesian components of the displacement vector can be separated and individually recorded by holographic interferometric techniques (Sciammarella and Gilbert, 1976). These methods have been complemented by powerful image processing techniques and, during the past decade, considerable research has been devoted toward facilitating computer-based holographic interferometric techniques for quantitative measurements of displacement and strain fields of deforming bodies, making them an effective tool for experimental stress analysis (Sciammarella and Ahmadshahi, 1984, 1986, 1988). Further advances in this field have led to what is known as electronic speckle-pattern interferometry, sometimes referred to as electronic holography (Stetson and Brohinsky, 1985).

Speckle-pattern interferometry, be it holographic or pho-

[1]Presently, Senior Engineer, C. E. Niehoff & Co., 2021 Lee Street, Evanston, IL 60202.

[2]Presently, Assistant Professor, Department of Mechanical Engineering, Northwestern University, Evanston, IL 60208-3020.

Contributed by the Applied Mechanics Division of THE AMERICAN SOCIETY OF MECHANICAL ENGINEERS for presentation at the ASME Winter Annual Meeting, New Orleans, LA, Nov. 28-Dec. 3, 1993.

Discussion on this paper should be addressed to the Technical Editor, Professor Lewis T. Wheeler, Department of Mechanical Engineering, University of Houston, Houston, TX 77204-4792, and will be accepted until four months after final publication of the paper itself in the ASME JOURNAL OF APPLIED MECHANICS.

Manuscript received by the ASME Applied Mechanics Division, June 26, 1991; final revision, Oct. 7, 1992. Associate Technical Editor: M. E. Fourney.

Paper No. 93-WA/APM-17.

Copies of this paper will be available until Mar. 1995.

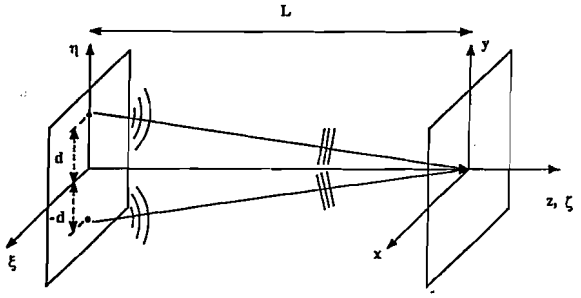

Fig. 1 Two point sources located on the ξ, η-plane; the x, y-plane lies on the photographic emulsion plate

tographic, has until now been limited to the study of static deformations, or at most, periodic deformations which occur when an object is under steady-state vibration. In the latter case, temporal modulation of the amplitude and/or phase of the illuminating lightwave (Aleksoff, 1971; and Ahmadshahi, 1988) has made full-field quantitative measurements of displacement and strain of vibrating bodies possible. However, in view of many technical problems, it has been stated as recently as 1989 that "dynamic speckle-pattern interferometry is not possible" (see Jones and Wykes, 1989). Although there are in principle no inherent limitations preventing the use of such techniques to record transient deformation, a number of technical difficulties must be overcome before dynamic speckle interferometry becomes a viable technique. Among these, intensity, resolution, and perhaps most importantly, image registration, have accounted for the preclusion of speckle techniques in the study of transient deformations until now.

In this paper, we discuss the development of dynamic holographic-electronic speckle-pattern interferometry and its application to analyze the deformations of diffusely reflecting bodies under transient loads. The objective of this research is to show that holographic speckle interferometry is applicable to dynamic problems, and more importantly, to demonstrate how this technique can be realized. Other optical methods, such as photoelasticity (Dally, Riley, and Durelli, 1959; Dally, Durelli and Riley, 1960; Durelli and Riley, 1961) and moiré (Riley and Durelli, 1962; Huntley and Field, 1989), have been employed with considerable success for dynamic stress and displacement analysis. However, they have many limitations. Michelson interferometry and some shearing interferometers (Krishnaswamy, Tippur, and Rosakis, 1992) require that the material be either transparent or, when it is opaque, be highly polishable. Photoelastic studies can only be performed on transparent, birefringent materials. It is further limited because auxiliary information is needed for the separation of the principal stresses. Moiré methods utilize gratings that need to be ruled, etched, or embedded onto the specimen and thus do not qualify as nondestructive testing techniques. Even in those circumstances where gratings with minimal surface intrusion are used, elevated temperature may compromise the integrity of the grating.

The technique described in this paper is complementary to the existing optical techniques in that it makes possible full-field, nondestructive, time-sequence measurements of components of the surface displacements of deforming bodies which are opaque and whose surfaces may not be polishable or which may degrade with temperature. The proposed method of dynamic holographic-electronic speckle-pattern interferometry can therefore be a valuable tool in the analysis of structural and/or material behavior over a relatively wide range of deformation rates and temperatures.

In the following sections, the principles of holographic speckle interferometry and the requirements of speckle correlation are first briefly outlined to lay the basis for the subsequent description of the proposed technique.

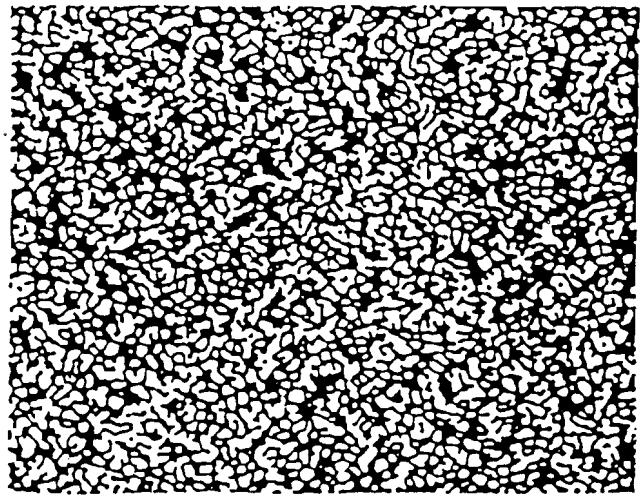

Fig. 2 Photograph of a typical speckle pattern

2 Holographic Speckle-Pattern Interferometry

Consider two point sources located on the ξ, η-plane which are mutually coherent, linearly polarized, and are emitting light waves of wavelength λ; (Fig. 1). If the x, y-plane (photographic emulsion plane) is relatively far from the ξ, η-plane, the optical field on this plane is the sum of two plane waves, and the intensity recorded by the photographic emulsion is in the form of sinusoidal fringes, the orientation and spatial frequency of which depend on the location of the points on the ξ, η-plane, the distance L, and the wavelength λ (Smith, 1969). The presence of a third point will result in recording the sum of three different sinusoidal fringes with different orientations and spatial frequencies. This is due to interference between point 1 and point 2, point 1 and point 3, and point 2 and point 3. Introducing a fourth point source on the ξ, η-plane will lead to an intensity distribution which is the sum of the intensities of six different sinusoidal fringe patterns with distinct spatial frequencies and orientations. If, now, the ξ, η-plane is taken as a rough (diffuse) surface which is being illuminated by a coherent light source, according to Huygen's principle, each point on the surface acts as a point source similar to those shown in Fig. 1. The collection of the optical field of all such points on the photographic emulsion medium gives rise to a random intensity distribution known as the speckle pattern; (see Fig. 2 and Dainty (1975)). For those who are involved with the study of deformations of solids, a speckle pattern can be thought of as a collection of fictitious marks on the surface of the specimen, and holographic interferometry is a process of monitoring their displacements.

In typical off-axis holographic interferometry (Leith and Upatnieks, 1962; and Sciammarella, 1982) two speckle patterns are recorded on the same photographic emulsion medium. Furthermore, these speckle patterns are holographic; that is, the optical setup includes a reference beam and/or a double illumination of the surface of the object. We will consider the latter case in which two mutually coherent collimated beams illuminate the surface of the object. The corresponding scattered wavefronts, W_1 and W_2, are simultaneously recorded on the film (Fig. 3). The electric fields of W_1 and W_2 at the film plane can be expressed as

$$E_1(x,y) = A(x,y)\exp[i\psi_1(x,y)], \tag{1}$$

$$E_2(x,y) = B(x,y)\exp[i\psi_2(x,y)]. \tag{2}$$

The recorded intensity then becomes

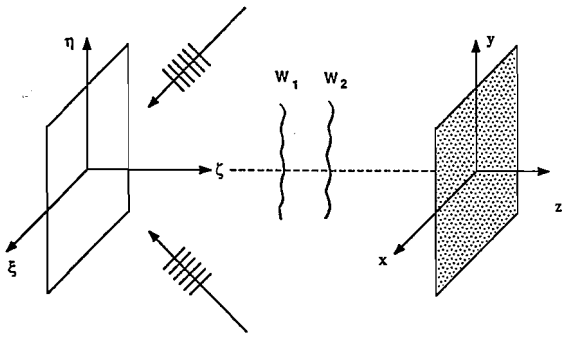

Fig. 3 Double illumination of a diffused surface

$$I_1(x,y) = \int_{-T/2}^{T/2} [E_1(x,y) + E_2(x,y)][\bar{E}_1(x,y) + \bar{E}_2(x,y)]dt,$$

$$= T\{A^2(x,y) + B^2(x,y) + 2A(x,y)B(x,y)\cos[\psi(x,y)]\}, \quad (3)$$

where

$$\psi(x,y) = \psi_1(x,y) - \psi_2(x,y), \quad (4)$$

an overbar indicates the complex conjugate; T is the time interval during which the film is exposed; $A(x, y)$ and $B(x, y)$ are amplitudes, and $\psi_1(x, y)$ and $\psi_2(x, y)$ are the phases (related to the random height variations of the points on the surface) of the two scattered wavefronts; and $i = \sqrt{-1}$. A second speckle pattern is recorded after the body has been deformed, and its intensity distribution is recorded as

$$I_2(x,y) = T\{A^2(x,y) + B^2(x,y) + 2A(x,y)B(x,y) \times \cos[\psi(x,y) + (\mathbf{K}_1 - \mathbf{K}_2)\cdot\mathbf{d}(\mathbf{x},\mathbf{y})]\}. \quad (5)$$

The sum of the two speckle patterns produces holographic interferometric fringes,

$$I(x,y) = I_1(x,y) + I_2(x,y),$$

or

$$I(x,y) = T\{2[A^2(x,y) + B^2(x,y)] + 4A(x,y)B(x,y) \times \cos[\psi(x,y) + (1/2)(\mathbf{K}_1 - \mathbf{K}_2)\cdot\mathbf{d}(\mathbf{x},\mathbf{y})] \times \cos[(1/2)(\mathbf{K}_1 - \mathbf{K}_2)\cdot\mathbf{d}(\mathbf{x},\mathbf{y})]\}, \quad (6)$$

with $\mathbf{K}_1$ and $\mathbf{K}_2$ representing the two illumination vectors (Solid, 1969) and $\mathbf{d}(\mathbf{x}, \mathbf{y})$ is the displacement vector. The corresponding scalar quantities K and $d(x, y)$ represent the magnitude of the difference between the illumination vectors, and the projection of the displacement vector in the corresponding direction, respectively. In Eq. (6), the first term in the right-hand side is the background intensity and the second term is composed of two sinusoidal parts: one part contains information regarding both surface roughness and deformation while the other part is related only to deformation of the object. It is this term that dramatically displays the fringe pattern seen in double exposure holography. Separate in-plane components of the displacement vector can be obtained by symmetric illumination of the object (Sciammarella and Gilbert, 1976), if the sensitivity vectors lie on the x, z and y, z-planes (Fig. 3); and the corresponding fringe patterns are then proportional to the x and y-components of the displacement vector, respectively.

3 Speckle Correlation

Experimentalists who employ the holographic interferometry technique to study object deformations are well aware of the stability requirements of the optical setup, and the recording medium in particular. Any small disturbance to the photographic emulsion medium will result in degradation of the contrast of the fringe pattern, to the extent that rigid-body motions of the hologram plane of the order of microns, could diminish them altogether. This behavior can be explained if we consider Eqs. (3) and (6), which are the speckle patterns before and after deformation. Suppose that before recording the second exposure, there is a rigid-body translation of the photographic recording medium by an amount x_0 and y_0, in the x and y-directions, respectively. Then Eq. (5) would take on the following form:

$$I_2(x,y) = T\{A^2(x,y) + B^2(x,y) + 2A(x,y)B(x,y) \times \cos[\psi(x-x_0,y-y_0) + Kd(x,y)]\}. \quad (7)$$

In Eq. (7), we have assumed that $A(x, y)$, $B(x, y)$, and $d(x, y)$ are all relatively slowly varying functions. Consequently, small shifts of the amount x_0 or y_0 will not change their form. The only term, however, that should be considered is the function $\psi(x, y)$, which is randomly varying and proportional to the roughness. Thus it changes completely, if small shifts are introduced. Finally, if the two speckle patterns of Eqs. (3) and (7) are added, the resulting intensity distribution will be

$$I(x,y) = T\{2[A^2(x,y) + B^2(x,y)] + 4A(x,y)B(x,y) \times \cos[(1/2)[\psi(x,y) + \psi(x-x_0,y-y_0) + Kd(x,y)] \times \cos[(1/2)[\psi(x,y) - \psi(x-x_0,y-y_0) + Kd(x,y)]\}. \quad (8)$$

In Eq. (8), the difference between $\psi(x, y)$ and its shifted version (the last line of the equation) is another random function which will overwhelm the term $Kd(x, y)$, and thus no discernible fringes can be seen if such rigid-body translations occur. One can see, therefore, that holographic interferometric fringes are formed only when the speckle patterns corresponding to the undeformed and deformed states of the object are well aligned, and fringe contrast strongly depends on how precisely the two speckle patterns are correlated.

4 Recording Dynamic Speckle Patterns

The principle of the DHESPI (Dynamic Holographic-Electronic Speckle-Pattern Interferometry) technique is based on recording a sequence of holographic speckle patterns on a photographic emulsion medium using a high-speed camera, and subsequently digitizing the negatives by means of a CCD camera and an image processing system. The digitized speckle patterns are then registered utilizing image correlation techniques. A reference speckle pattern corresponding to the undeformed (or a suitable preceding deformed) state of the object is subtracted from the remaining speckle patterns which are obtained during subsequent deformation.

Figure 4 illustrates the dynamic recording of time-varying speckle patterns using a high-speed camera (Cordin model 330A) and an image processing system. The scattered waves due to double illumination of the object are recorded by the high-speed camera as a sequence of snapshots on T-Max P3200 Kodak film. The electric field due to the scattered waves at the film plane is

$$E(x,y,t) = E_1(x,y,t) + E_2(x,y,t) = A(x,y,t)\exp[i\psi_{T1}(x,y,t)] + B(x,y,t)\exp[i\psi_{T2}(x,y,t)], \quad (9)$$

$$\psi_{T1}(x,y,t) = \psi_1(x,y) + (K_1 - K_0)d(x,y,t), \quad (10)$$

$$\psi_{T2}(x,y,t) = \psi_2(x,y) + (K_2 - K_0)d(x,y,t), \quad (11)$$

where $(K_1 - K_0)$ and $(K_2 - K_0)$ are sensitivity constants and $d(x, y)$ is a component of the displacement vector in the direction of the sensitivity vectors. We will postpone to the next section the description of the procedure to separate and individually obtain the three components of the displacement vector.

The sequence of exposures obtained by the high-speed camera can be analyzed best through the use of a shuttering se-

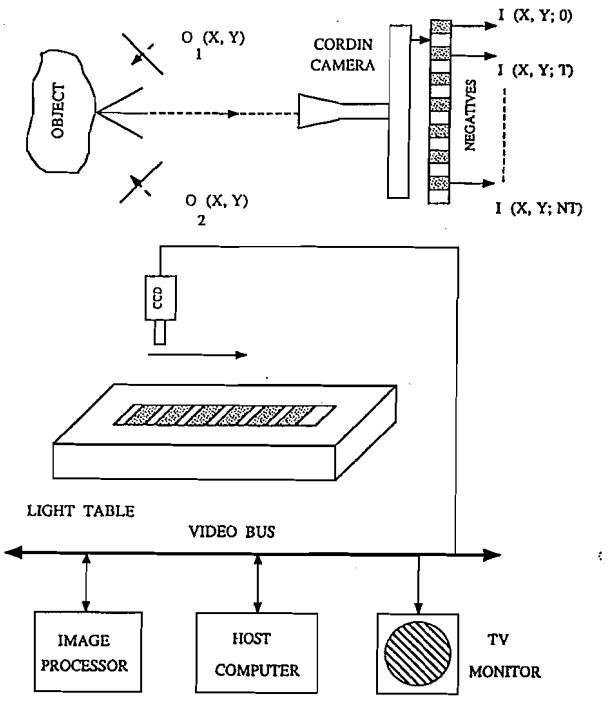

Fig. 4 Schematic representation of dynamic recording of time-varying speckle patterns, and the image processing system

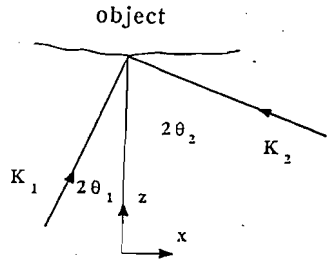

Fig. 5 Schematic representation of double illumination beams and the corresponding illumination vectors

quence $S_n(t; T)$, where T is the period of the shutter sequence and the index n signifies the elements of the sequence. The intensity distribution of each negative is then

$$I_1(x,y;nT) = \int_{-\infty}^{\infty} E(x,y,t) \times \bar{E}(x,y,t) \times S_n(t;T)dt,$$

$$n = 0, 1, 2, 3, \ldots, N, \quad (12)$$

where the elements of the sequence $\{S_n\}$ are functions such that

$$S_n(t;T) = \begin{cases} n\text{th arbitrary function} & 0 \le t \le T \\ 0 & \text{otherwise.} \end{cases} \quad (13)$$

The most useful function, achieved through the on-off switching of the light source, is the Dirac-Delta distribution, i.e.,

$$S_n(t;T) = \delta(t - nT) \quad n = 0, 1, 2, 3, \ldots, N, \quad (14)$$

so that each of the $N + 1$ arbitrary functions is an impulse and that they differ only by a shift in time. Therefore, the sequence of intensity distributions is

$$I(x,y;nT) = E(x,y,nT) \times \bar{E}(x,y,nT)$$
$$= [A^2(x,y,nT) + B^2(x,y,nT) + 2A(x,y,nT)$$
$$\times B(x,y,nT)\cos[\psi(x,y) + (K_1 - K_2)d(x,y,nT)]$$
$$n = 0, 1, 2, 3, \ldots, N \quad (15)$$

with $\psi(x, y)$ defined by Eq. (4). These intensity distributions are digitized and stored by the image processing system to be correlated and reconstructed to produce time-varying fringe patterns.

5 Quantitative Measurement

The information carried by the speckle pattern of Eq. (15) relates to the surface roughness and a component of the displacement vector. The corresponding in-plane components can be obtained in the following manner. Consider the case where the propagation vectors of the two collimated illumination beams lie on the x, z-plane (Fig. 5) and are written as

$$\mathbf{K}_1 = \frac{2\pi}{\lambda}(\sin 2\theta_1 \mathbf{e}_x + \cos 2\theta_1 \mathbf{e}_z), \quad (16)$$

$$\mathbf{K}_2 = \frac{2\pi}{\lambda}(-\sin 2\theta_2 \mathbf{e}_x + \cos 2\theta_2 \mathbf{e}_z), \quad (17)$$

where $2\theta_1$ and $2\theta_2$ are the angles between the illumination vectors and the z-axis, taking on only positive values. The object displacement vector at any point in space and time is written as

$$\mathbf{d}(x,y,t) = u(x,y,t)\mathbf{e}_x + v(x,y,t)\mathbf{e}_y + w(x,y,t)\mathbf{e}_z, \quad (18)$$

where $u(x, y, t)$ and $v(x, y, t)$ are the in-plane and $w(x, y, t)$ the out-of-plane displacement components. Furthermore, the displacement vector at $t = 0$, corresponding to the undeformed state of the object, is taken as zero,

$$\mathbf{d}(x,y,0) = \mathbf{0}. \quad (19)$$

The digitized speckle patterns obtained from the intensity distributions recorded on the film are then correlated and, as in the case of ESPI (Electronic Speckle-Pattern Interferometry), subtracted in order to generate holographic interferometric fringes. The recorded speckle pattern corresponding to time $t = 0$ is selected as the reference image and subsequent images are subtracted from it, which results in a sequence of intensity distributions as

$$q(x,y;nT) = I(x,y;nT) - I(x,y;0), \quad n = 1, 2, 3, \ldots, N. \quad (20)$$

For example, if we consider the case where the illumination vectors lie on the x, z-plane, the speckle-pattern intensity distribution can be represented as

$$I(x,y;nT) = [A^2(x,y) + B^2(x,y)] + 2A(x,y)$$
$$\times B(x,y)\{\cos[\psi(x,y) + k_x u(x,y,nT)$$
$$+ k_z w(x,y,nT)]\}, \quad n = 0, 1, 2, 3, \ldots, N, \quad (21)$$

where

$$k_x = \frac{\pi}{\lambda}(\sin 2\theta_1 + \sin 2\theta_2), \quad (22)$$

$$k_z = \frac{\pi}{\lambda}(\cos 2\theta_1 - \cos 2\theta_2). \quad (23)$$

In this way Eq. (20) can be expanded to give

$$q(x,y;nT) = 4A(x,y)B(x,y) \times \sin[\psi(x,y) + k_x u(x,y,nT)$$
$$+ k_z w(x,y,nT)] \times \sin[k_x u(x,y,nT) + k_z w(x,y,nT)],$$
$$n = 1, 2, 3, \ldots, N. \quad (24)$$

Symmetric illumination of the specimen ($2\theta_1 = 2\theta_2$) results in

$$q(x,y;nT) = 4A(x,y)B(x,y) \times \sin[k_x u(x,y,nT)]$$
$$\times \sin[\psi(x,y) + k_x u(x,y,nT)], \quad n = 1, 2, 3, \ldots, N. \quad (25)$$

Similar results can be obtained for the other in-plane component of the displacement vector, if we symmetrically illuminate the specimen such that the propagation vectors lie on the y, z-plane,

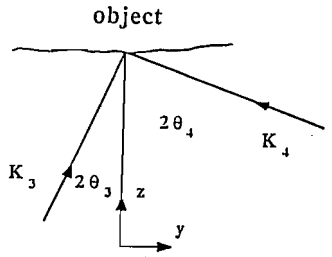

Fig. 6 Schematic representation of double illumination beams and the corresponding illumination vectors

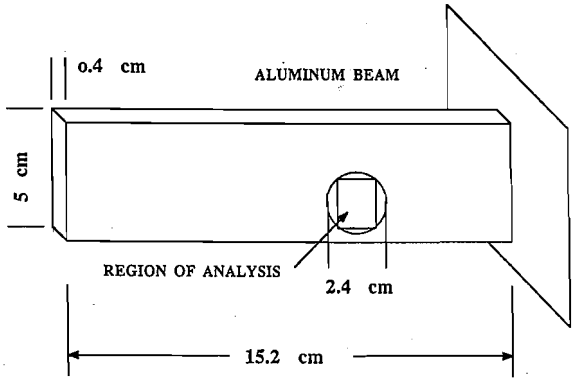

Fig. 7 Cantilever beam and the region of analysis

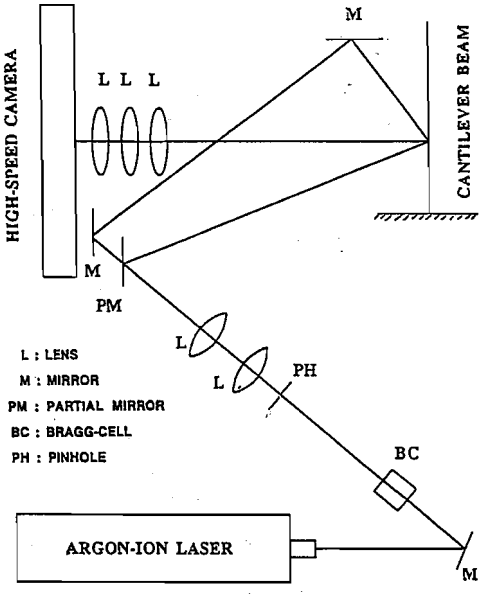

Fig. 8 Optical setup

$$q(x,y;nT) = 4A(x,y)B(x,y) \times \sin[k_y v(x,y,nT)] \times \sin[\psi(x,y) + k_y v(x,y,nT)], \quad n = 1, 2, 3, \ldots, N, \quad (26)$$

with

$$k_y = \frac{\pi}{\lambda}(\sin 2\theta_3 + \sin 2\theta_3) = \frac{2\pi}{\gamma} \sin 2\theta_3 \quad (27)$$

It should be mentioned that, although some of the above equations are limited to small deformations, large deformations can also be accommodated by an incremental method. That is, consecutive pairs of speckle patterns may be subtracted, instead of using the initial speckle pattern as the reference, to generate the interferometric fringes, and the total displacement would be obtained by the addition of all the corresponding increments.

6 Experiment

To demonstrate the feasibility of the technique, the proposed method was used to get a time sequence of a periodically deforming object in order to enable direct comparison with conventional stroboscopic speckle methods. This is essential to gain confidence in the technique prior to using it to recover truly transient deformation. Thus the time evolution of the displacement of a vibrating cantilever beam at resonance is studied. The aluminum cantilever beam is 15.2 cm long, 5 cm wide, and 0.4 cm thick (Fig. 7). An argon-ion cw laser is used as the light source which delivers 1.2 w/cm^2 power. Laser intensity limitations restrict the field of analysis to a rectangular region inscribed in a circular region 2.4 cm in diameter, as shown in Fig. 7. The cantilever beam is excited by an electromagnetic shaker. At a frequency of 3125 Hz, a plate-mode resonance is detected. The optical setup is shown in Fig. 8. The laser beam is passed through a Bragg-Cell, which provides a flash of light equal to 3.2 ms. This period is long enough to expose 80 frames of the high-speed camera which was set to operate at 25,000 frames per second. This corresponds to exposure and interframe times of 20 μs each. The beam is then passed through a pinhole and two well-corrected lenses of 175 mm focal length, to produce a collimated beam 2.4 cm in diameter. This beam is passed through a 50/50 partial mirror, providing two equal intensity collimated beams, one of which illuminates the cantilever beam at an angle of 20 deg with the normal, and the other at an angle of 55 deg with the normal; Fig. 8. The region is imaged onto the film track of the high-speed camera by its internal lens system and three well-corrected lenses of 381 mm, 381 mm, and 175 mm focal lengths, as shown in Fig. 8. The recording medium, T-MAX P3200 Kodak film, is reported by the manufacturer to have a resolution of approximately 40 l/mm. The high-speed Cordin camera used in this experiment is capable of at least the same resolving power since its resolution is reported to be 40 l/mm at a speed of 2,000,000 frame per second. Therefore, it is expected that at lower speeds, specifically 25,000 frames per second used in this experiment, the resolution of the camera is considerably higher than the film, and consequently, it is the film that determines the spatial resolution of the system. One of the internal relay lenses of the camera has a focal distance of approximately 300 mm, and an effective aperture was taken to be the width of the beam-splitting cube of the camera which was 8.5 mm. This gives a speckle size of roughly 20 μ. As mentioned previously, the illuminations were not symmetric, so that the fringe patterns are due to a combination of in-plane and out-of-plane displacement components. Utilizing Eqs. (22) and (23) we get for the sensitivity constants K_x and K_z the values of 9.67 rad/μ and 6.77 rad/μ, respectively. The modulus of the resulting sensitivity vector is then, K = 11.8 rad/μ and the corresponding direction of approximately Θ_k = 35 deg. Therefore, the fringes can be thought of as representing the component of the displacement vector, making an angle of 35 deg to the normal of the cantilever beam, and each fringe corresponds to 0.53 μ of this displacement.

7 Results

Figure 9 shows the time-frozen fringes of the vibrating beam corresponding to the maximum displacement, using ESPI and strobing technique. This was intended to verify the dynamic analysis of the subregion shown in the same figure. Figure 10 shows the sinusoidal amplitude of the time-varying displacement which can be written as

$$w(x,y,t) = \cos(2\pi\Omega t) f(x,y), \quad (28)$$

where Ω = 3215 Hz, and $f(x, y)$ is the mode shape whose interferometric fringe pattern is shown in Fig. 9.

The experiment is conducted in such a way that while the

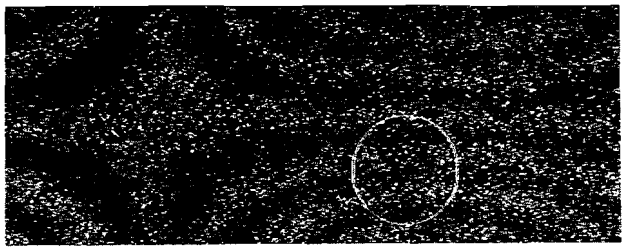

Fig. 9 Time-frozen fringes corresponding to the maximum displacement using electronic speckle-pattern interferometry and strobing technique; the evolution of fringe pattern in the rectangular subregion is studied by dynamic holographic-electronic speckle-pattern interferometry

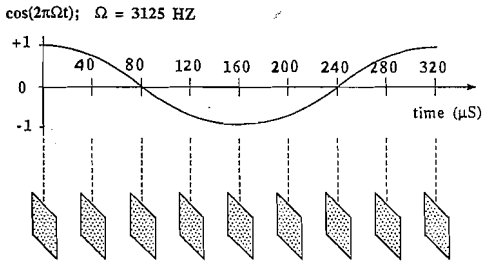

Fig. 10 Time-varying amplitude of the mode function; dotted parallelograms are schematic representations of the holographic speckle patterns obtained at discrete times using a high-speed camera

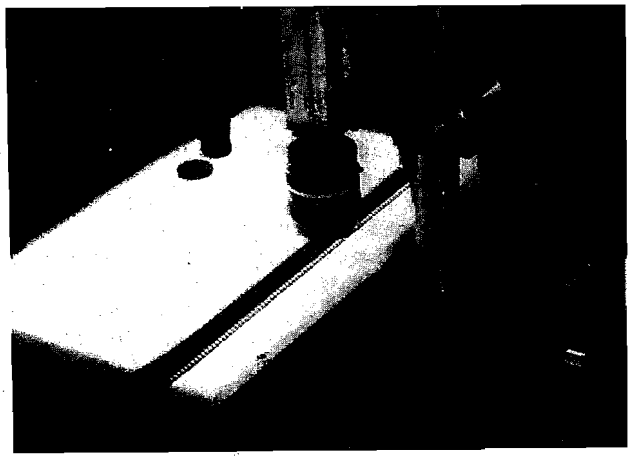

Fig. 11 Image digitization system

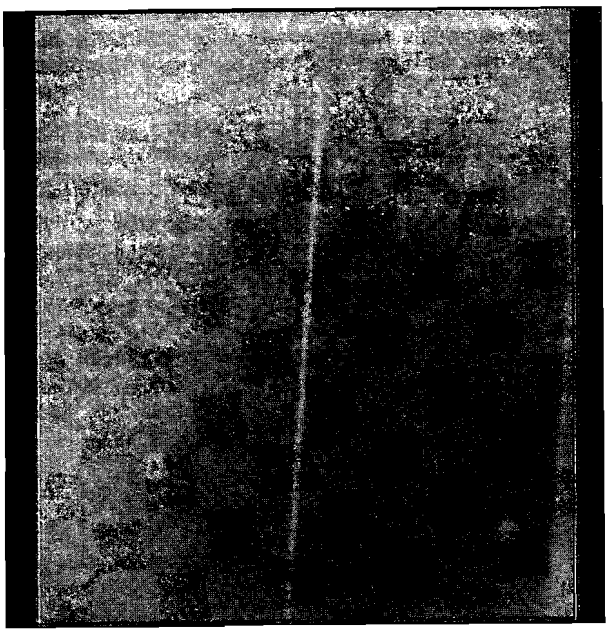

Fig. 12 Holographic speckle pattern obtained at $t = 0$ μs

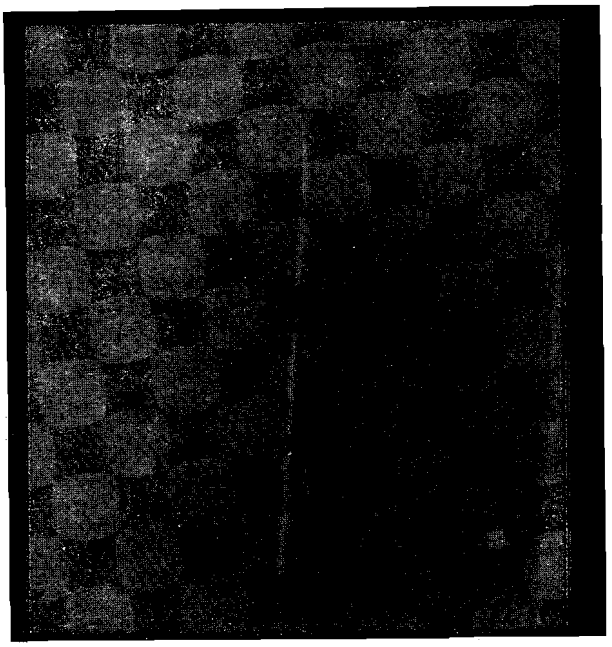

Fig. 13 Holographic speckle pattern obtained at $t = 40$ μs

cantilever beam is vibrating and the rotating mirror of the high-speed camera is rotating, a pulse of light of period 3.2 μs is applied by the Bragg-Cell, corresponding to 80 frames, eight of which are sufficient to complete one cycle of vibration. Taking the first exposure frame at the maximum or the minimum of the amplitude of vibration (of which we have chosen the former), the deformation during the subsequent one-half cycle of vibration is analyzed. It should be noted that the two illumination beams, as described in Section 6, are not symmetric, and thus, both components $u(x, y, t)$ and $w(x, y, t)$ contribute to the total phase, Eq. (24). This is because symmetric illumination annihilates the term $w(x, y, t)$, and the displacement component $u(x, y, t)$ alone could not produce a sufficient number of fringes in the subregion shown in Fig. 9. This is expected since the thickness of the cantilever beam is small compared to its other dimensions, and, therefore, membrane deflections are much higher in magnitude than in-plane stretches. Hence the fringes obtained and shown in what follows are predominantly due to the out-of-plane displacement component.

Figure 11 shows the setup used to digitize the negatives. A CCD camera and an image processing system are used to digitize the developed negatives, mounted on a light table. Careful registration of the negatives is accomplished by (1) marking the specimen with three noncollinear dots at arbitrary locations, for course alignment; (2) mounting the CCD camera on a translation stage (Newport model 400) for fine alignment; and, finally, (3) by cross-correlation of the digital images.

Figures 12 and 13 show two digitized speckle patterns corresponding to $t = 0$ μs and $t = 40$ μs, respectively. After registration, the two images are subtracted and the results, obtained through the use of image processing techniques, is shown in Fig. 14. The intermediate processing stages leading to the final result involve: a 2-D low-pass filter, a narrow-band band-pass filtering in the vertical direction, followed by a narrow-band band-pass Hilbert transform combination filtering in the vertical direction to normalize the amplitude variation of the fringe pattern (Ahmadshahi, 1998). Figure 15 shows the

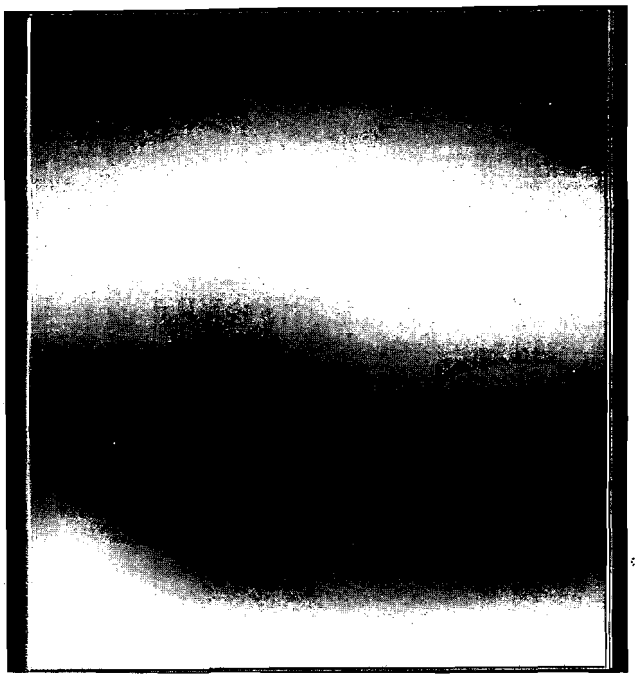

Fig. 14 Enhanced fringe pattern obtained by subtracting the image shown in Fig. 13 from that shown in Fig. 12; the fringe pattern corresponds to the difference between the maximum displacement and the displacement 40 μs later in time

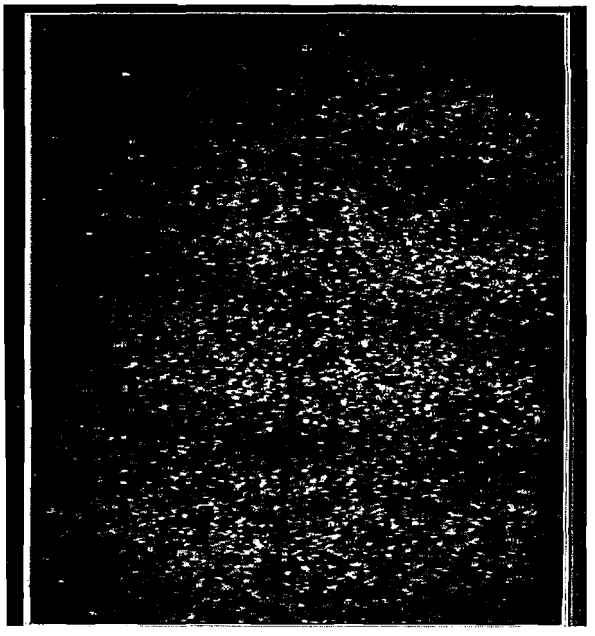

Fig. 15 The result of subtraction of two holographic speckle patterns obtained at $t = 0$ μs and $t = 120$ μs

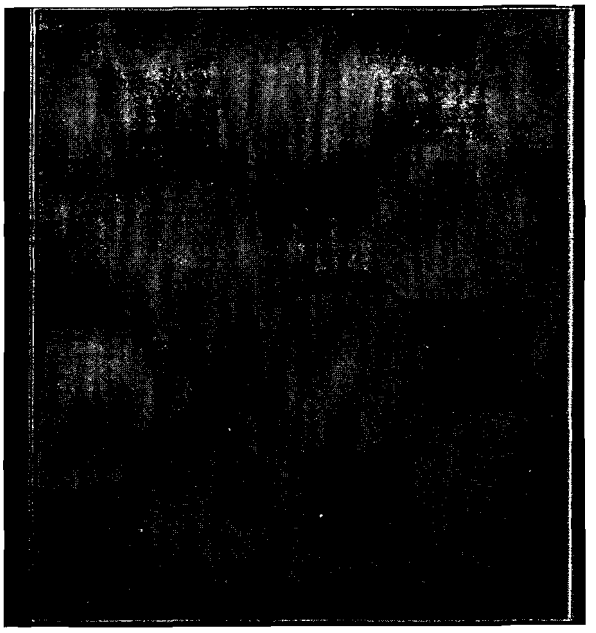

Fig. 16 The result of 2-D band-pass filter applied to Fig. 15

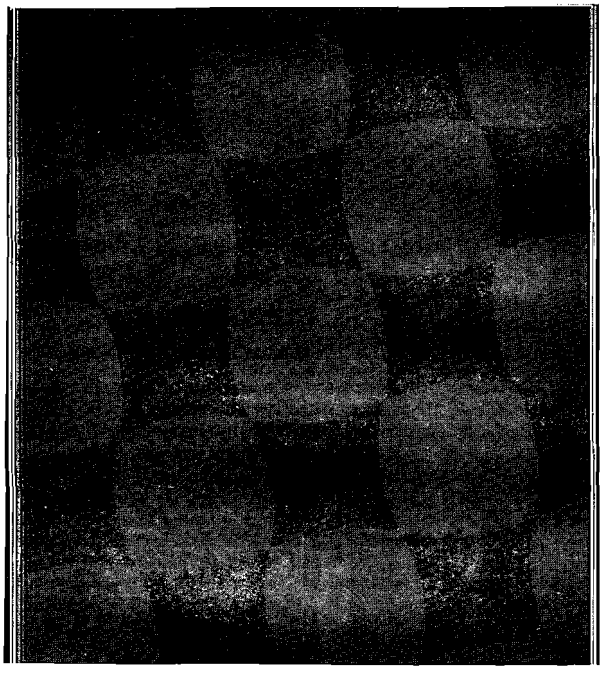

Fig. 17 The result of 1-D low-pass filter applied in the horizontal direction to Fig. 16

result of subtraction of the digitized speckle pattern corresponding to $t = 120$ μs from that obtained at $t = 0$ μs. Figure 16 shows the result of 2-D low-pass and a 1-D narrow-band band-pass filtering of the image shown in Fig. 15. Figure 17 shows the result of 1-D narrow-band low-pass filtering applied in the horizontal direction to Fig. 16. Finally, this image is normalized by generating an in-quadrature image using a combination of a narrow-band band-pass filter and a narrow-band band-pass Hilbert transform; Fig. 18. All 1-D filters are of finite-impulse-response linear-phase type, and their band-pass widths are ± 1 harmonic around the central frequency based on a 512 pixel resolution. Typical filter length is 101 samples. Figure 19 is the composite image of the evolution of the fringe pattern during 160 μs. The figure represents the subtracted speckle patterns obtained at $t = 40$ μs, $t = 80$ μs, $t = 120$ μs and $t = 160$ μs, from the reference speckle pattern obtained at $t = 0$ μs.

It is not possible to directly ascertain the accuracy of our results, since we have no theoretical solution to this particular problem. Furthermore, because of the asymmetric illumination of the specimen, the obtained fringe patterns are a combination of the in-plane and the out-of-plane components of the displacement vector. Consequently, we have adopted a consistency test and the accuracy of the results will be based upon how consistent the fringe patterns are with respect to each other. Specifically, we have chosen the fringe pattern corresponding to deformation at $t = 120$ μs as the base image to obtain the mode shape as given in Eq. (28). This is because

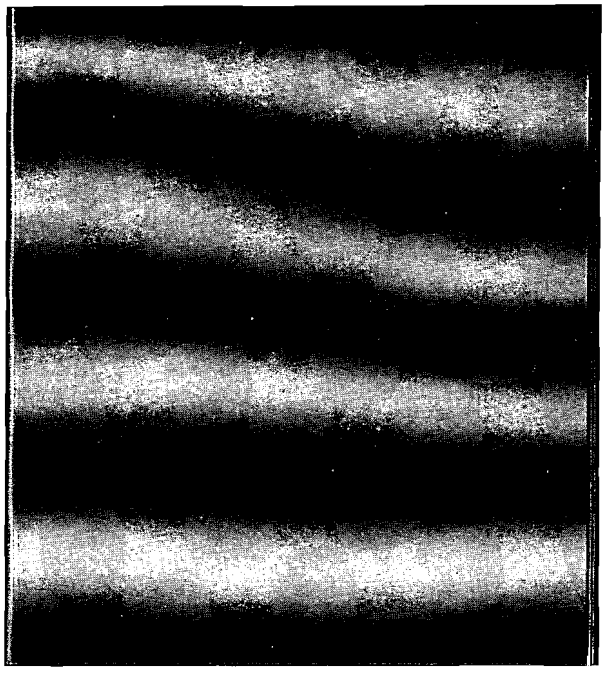

Fig. 18 Normalized fringes

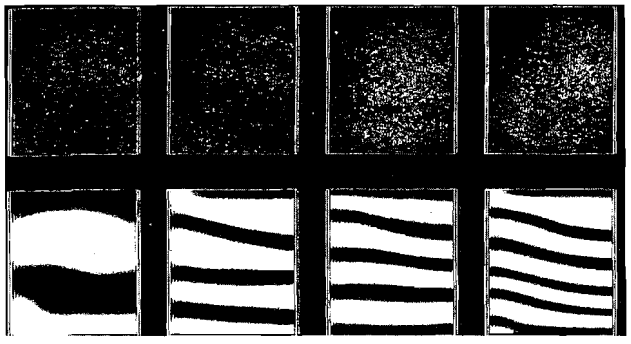

Fig. 19 Evolution of displacement in a rectangular subregion of a cantilever beam during 1/2 cycle of vibration obtained at t = 40 μs, t = 80 μs, t = 120 μs, and t = 160 μs, from the reference obtained at t = 0 μs

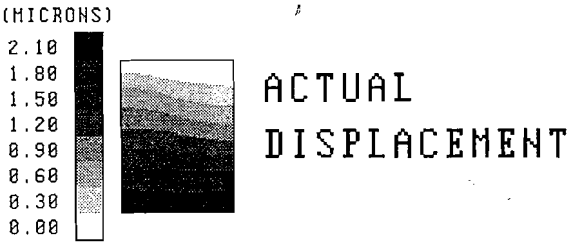

Fig. 20 Actual displacement levels obtained from the fringe patterns at t = 120 μs

the signal-to-noise ratio of this image was found to be the highest compared to the other three fringe patterns. Figure 20 shows the levels of displacements obtained from the fringe patterns shown in Fig. 18. Figures 21–23 show the comparison between the "actual" displacements and the "compared" displacements occurring at t = 40 μs, t = 80 μs, t = 160 μs, and the corresponding absolute errors. By "actual" displacement we mean those calculated from the fringe patterns corresponding to t = 40 μs, t = 80 μs, t = 160 μs. The "compared" displacements are simply those obtained by multiplying the displacement levels of the base image at t = 120 μs, Fig. 20, by the appropriate time-dependent factors (obtained from Eq. (28)) which are 0.41, 0.59, and 1.18, respectively.

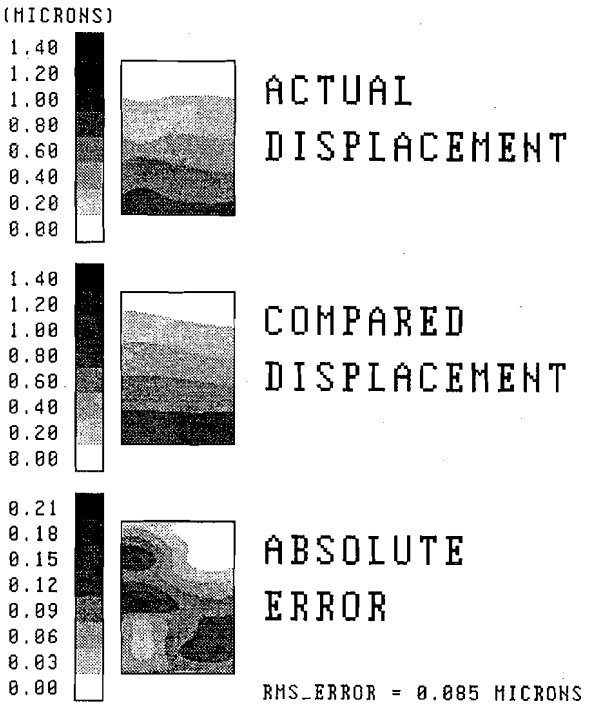

Fig. 21 Actual displacements obtained from the fringe pattern at t = 40 μs compared for consistency with the displacements expected from appropriate time-dependent scaling of the base image at t = 120 μs

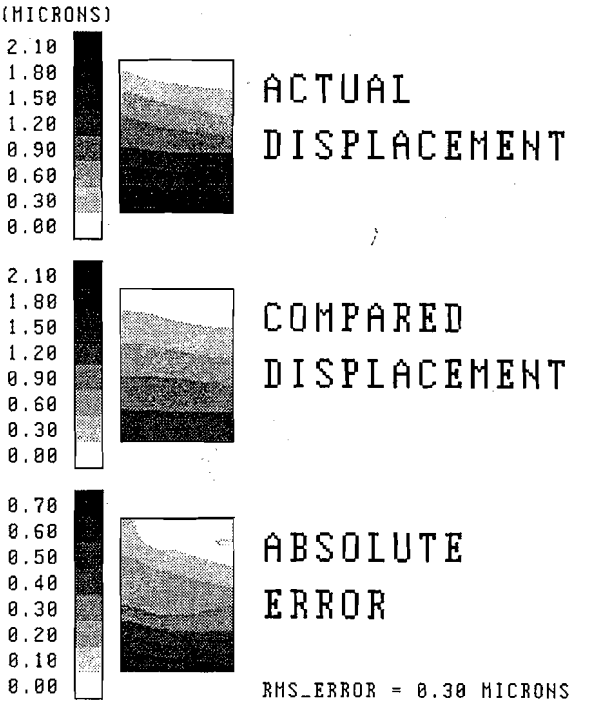

Fig. 22 Actual displacements obtained from the fringe pattern at t = 80 μs compared for consistency with the displacements expected from appropriate time-dependent scaling of the base image at t = 120 μs

It is observed that the main contribution to the absolute error arises from the edges and the corners of the images. This is most likely due to the well-known edge distortions associated with discretized and finite length convolution operations used in the image processing. Furthermore, relatively long exposure times (20 μs for each frame) are likely to introduce additional errors, since the fringe patterns involve some time-averaging, and therefore are not the sinusoidal ones which govern the

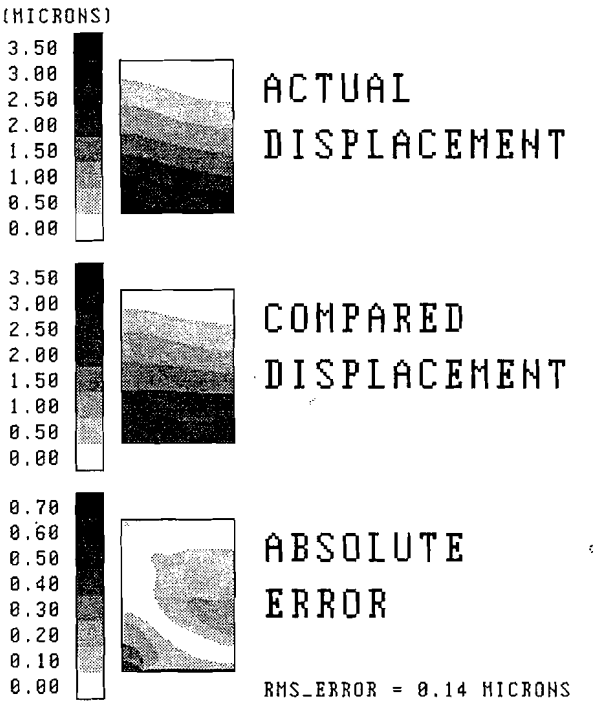

Fig. 23 Actual displacements obtained from the fringe pattern at t = 160 μs compared for consistency with the displacements expected from appropriate time-dependent scaling of the base image at t = 120 μs

static or stroboscopic interferometric fringes. This error can be minimized by reducing the exposure time of each frame via synchronized ultra-short-duration laser pulses of sufficiently high power.

8 Conclusions

A nondestructive optical technique to quantitatively study the full-field transient deformation of diffusely reflecting bodies is reported in this paper. The technique is a two-step process, whereby a sequence of holographic speckle patterns generated by doubly illuminating the surface of the specimen is first recorded by means of a high-speed camera during deformation of the object, and the developed negatives containing the record of the dynamic speckle patterns are subsequently sequentially digitized by a CCD camera and an image processing system. A reference speckle pattern corresponding to the undeformed state of the object, is used to subtract the remaining speckle patterns from it, and the result has been shown to produce fringe patterns of the components of the time-varying displacement vector.

For illustration purposes, the technique is applied to the case of a vibrating cantilever beam, and the evolution, a combined in-plane and out-of-plane components of the displacement vector during one-half cycle of the vibration, is determined. It is shown, however, that due to nonperfect alignment of the digitized speckle patterns, the interferometric fringes produced by subtracting pairs of speckle patterns are of rather low contrast. Therefore, it is essential to employ image processing techniques to enhance the fringe contrast prior to making quantitative measurements.

The high-speed camera used in our experiment has the capability of operating at 2,000,000 frames per second. For 80 frames at this speed, the time resolution is 0.5 μs, and so events that last tens of a microseconds can be analyzed using DHESPI. Lack of laser intensity, however, currently limits our analysis to relatively small regions and long exposure times. Use of a pulsed laser might alleviate this problem, and then, for instance, detailed scrutiny of the displacement fields ahead of a rapidly moving crack can be studied through the use of Dynamic Holographic-Electronic Speckle-Pattern Interferometry in situations where other techniques may not be suitable.

9 Acknowledgments

The authors wish to recognize their colleague and dear friend, the late Dr. John E. Starrett, for his contributions to theoretical and practical aspects of this research. The technical assistance of Mr. David Lischer and Mr. Jon Isaacs is greatly appreciated. Thanks are also due to Mr. Abbas Azhdari for his help with the experiments.

This work has been supported by the U.S. Army Research Office under Contract No. DAAL-03-86-K-0169 with the University of California, San Diego.

References

Ahmadshahi, M. A., 1988, "Computer Based Techniques for Holographic Fringe Pattern Information Detection," Ph.D. Thesis, Illinois Institute of Technology.

Aleksoff, C. C., 1971, "Temporally Modulated Holography," *Appl. Opt.*, Vol. 10, No. 6, pp. 1329–1341.

Dainty, J. C., ed., 1975, *Laser Speckle and Related Phenomena*, Springer-Verlag, Berlin.

Dally, J. W., Durelli, A. J., and Riley, W. F., 1960, "Photoelastic Study of Stress Wave Propagation in Large Plates," *Proc. of SESA*, Vol. 17, pp. 33–50.

Dally, J. W., Riley, W. F., and Durelli, A. J., 1959, "A Photoelastic Approach to Transient Stress Problems Employing Low-Modulus Materials," ASME JOURNAL OF APPLIED MECHANICS, Vol. 26, Vol. 81, pp. 613–620.

Durelli, A. J., and Riley, W. F., 1961, "Stress Distribution on the Boundary of a Circular Hole in a Large Plate During Passage of a Stress Pulse of Long Duration," ASME JOURNAL OF APPLIED MECHANICS, Vol. 28, Vol. 83, pp. 245–251.

Francon, M., 1975, *Laser Speckle and Applications in Optics*, Academic Press, New York.

Gabor, D., 1948, *Nature*, Vol. 161, No. 4098, pp. 777–778.

Huntley, J. M., and Field, J. E., 1989, "High Resolution Moire Photography: Application to Dynamic Stress Analysis," *Opt. Eng.*, Vol. 28, No. 8, pp. 926–933.

Jones, R., and Wykes, C., 1989, *Holographic and Speckle Interferometry*, Cambridge University Press, Cambridge, U.K.

Krishnaswamy, S., Tippur, H. V., and Rosakis, A. J., 1992, "Measurement of Transient Crack Fields Using the Method of Coherent Gradient Sensing," *J. Mech. Phys. Solids*, Vol. 40, No. 2, pp. 339–372.

Leith, E. N., and Upatnieks, J., 1962, "Reconstructed Wavefronts and Communication Theory," *J. Opt. Soc. Amer.*, Vol. 52, pp. 1123–1130.

Riley, W. F., and Durelli, A. J., 1962, "Application of Moire Method to the Determination of Transient Stress and Strain Distribution," ASME JOURNAL OF APPLIED MECHANICS, Vol. 29, pp. 23–29.

Sciammarella, C. A., 1982, "Holographic Moire, an Optical Tool for the Determination of Displacements, Strains, Contours and Slopes of Surfaces," *Opt. Eng.*, Vol. 21, No. 3, pp. 447–457.

Sciammarella, C. A., and Ahmadshahi, M. A., 1984, "A Computer Based Method for Fringe Pattern Analysis," *Proc. of the 1984 SEM Fall Meeting*, pp. 61–69.

Sciammarella, C. A., and Ahmadshahi, M. A., 1986, "An Optoelectronic System for Fringe Pattern Analysis," *Exper. Tech.*, Vol. 10, No. 7, pp. 8–13.

Sciammarella, C. A., and Ahmadshahi, M. A., 1988, "A Computer Based Holographic Interferometry to Analyze 3-D Surfaces," *Proc. of IMEKO XI World Congress of the International Measurement Confederation*, pp. 167–175.

Sciammarella, C. A., and Gilbert, J. A., 1976, "A Holographic-Moire Technique to Obtain Separate Patterns for Components of Displacement," *Exper. Mech.*, Vol. 16, No. 6, pp. 215–220.

Smith, H. M., 1969, *Principles of Holography*, John Wiley and Sons, New York.

Solid, J. E., 1969, "Holographic Interferometry Applied to Measurements of Small Static Displacements of Diffusely Reflecting Surfaces," *Appl. Opt.*, Vol. 8, pp. 1587–1595.

Stetson, K. A., and Brohinsky, W. R., 1985, "Electronic Holography and Its Application to Hologram Interferometry," *Appl. Opt.*, Vol. 24, No. 21, pp. 3631–3637.

Printed in U.S.A.